RESEARCH ARTICLE

Key Points:
- The optimized total anthropogenic emissions were 1.5× higher than the a priori bottom-up inventory estimates
- Livestock and wetland sources represented 41% and 34% of total methane emissions, respectively
- The temporal variability of the regional emissions was dominated by wetlands with peak emissions occurring in August

Correspondence to:
Z. Chen and T. J. Griffis,
chen3274@umn.edu;
timgriffis@umn.edu

Source Partitioning of Methane Emissions and its Seasonality in the U.S. Midwest

Zichong Chen[1] [iD], Timothy J. Griffis[1] [iD], John M. Baker[1,2] [iD], Dylan B. Millet[1] [iD], Jeffrey D. Wood[3] [iD], Edward J. Dlugokencky[4] [iD], Arlyn E. Andrews[4] [iD], Colm Sweeney[4,5] [iD], Cheng Hu[1] [iD], and Randall K. Kolka[6]

[1]Department of Soil, Water, and Climate, University of Minnesota, St. Paul, MN, USA, [2]Agriculture Research Service, United States Department of Agriculture, St. Paul, MN, USA, [3]School of Natural Resources, University of Missouri, Columbia, MO, USA, [4]Global Monitoring Division, NOAA Earth System Research Laboratory, Boulder, CO, USA, [5]Cooperative Institute for Research in Environmental Sciences, University of Colorado Boulder, Boulder, CO, USA, [6]United States Department of Agriculture-Forest Service, Northern Research Station-Grand Rapids, Grand Rapids, MN, USA

Abstract The methane (CH_4) budget and its source partitioning are poorly constrained in the Midwestern United States. We used tall tower (185 m) aerodynamic flux measurements and atmospheric scale factor Bayesian inversions to constrain the monthly budget and to partition the total budget into natural (e.g., wetlands) and anthropogenic (e.g., livestock, waste, and natural gas) sources for the period June 2016 to September 2017. Aerodynamic flux observations indicated that the landscape was a CH_4 source with a mean annual CH_4 flux of $+13.7 \pm 0.34$ nmol m^{-2} s^{-1} and was rarely a net sink. The scale factor Bayesian inversion analyses revealed a mean annual source of $+12.3 \pm 2.1$ nmol m^{-2} s^{-1}. Flux partitioning revealed that the anthropogenic source (7.8 ± 1.6 Tg CH_4 yr^{-1}) was 1.5 times greater than the bottom-up gridded United States Environmental Protection Agency inventory, in which livestock and oil/gas sources were underestimated by 1.8-fold and 1.3-fold, respectively. Wetland emissions (4.0 ± 1.2 Tg CH_4 yr^{-1}) were the second largest source, accounting for 34% of the total budget. The temporal variability of total CH_4 emissions was dominated by wetlands with peak emissions occurring in August. In contrast, emissions from oil/gas and other anthropogenic sources showed relatively weak seasonality.

1. Introduction

The Midwestern United States is one of the most intensively managed agricultural regions in the world. This landscape is dominated by corn and soybean ecosystems that help support a livestock population of approximately 728 million animals within the U.S. Corn Belt (USDA NASS, 2014). This region is also one of the most wetland-rich landscapes across the United States (US Forest Service, 2016). In addition, it includes a variety of urban and industrial complexes and major oil refineries. Short-term methane (CH_4) measurements from a very tall tower within the region indicated that it is an important source of CH_4 (Zhang, Lee, Griffis, Baker, & Xiao, 2014). However, the CH_4 budget, its source partitioning, and seasonality remain poorly constrained.

Recent space-based measurements imply large uncertainties in the United States anthropogenic CH4 budget (Jacob et al., 2016; Kort et al., 2014; Turner et al., 2015; Wecht et al., 2014). Bottom-up inventory emission databases, such as EDGAR42 (Emission Database for Global Atmospheric Research, version 4.2, 2011, http://edgar.jrc.ec.europa.eu), show that enteric fermentation, natural gas production, and manure management represent the top three anthropogenic CH4 sources for the region. Miller et al. (2013) combined an atmospheric transport model and a geostatistical inverse modeling approach to estimate anthropogenic CH4 emissions across the U.S. for 2007 and 2008. They found that the CH4 budget in the United States was underestimated by 1.5 and 1.7 times in the EPA (U.S. Environmental Protection Agency, https://www.epa.gov/) and EDGAR42 inventories, respectively. This was largely attributed to underestimates of the livestock and natural gas emissions. Furthermore, Bruhwiler et al. (2017) also highlighted the large uncertainties of regional to continental scale CH4 emissions from using space-based observations, resulting from atmospheric transport variability, satellite sampling bias, and the choice of upwind background CH_4 concentration.

With the EDGAR42 bottom-up inventory used as a priori, Wecht et al. (2014) estimated North American CH4 emissions at high spatial resolution by inversions of SCIAMACHY satellite observations using the GEOS-Chem chemical transport model and its adjoint. They suggested that U.S. livestock emissions were 40% greater than

EDGAR42 and EPA inventories and that the low bias was associated with large underestimates in Iowa and Southern Minnesota. They also found that emissions associated with oil and gas were reasonably well-constrained by EPA. Turner et al. (2015) used 3 years of GOSAT satellite retrievals of column averaged CH_4 mole fraction (2009–2011) to constrain North American CH_4 emissions with high spatial resolution, with an inversion based on the GEOS-Chem adjoint. Their estimates of CH_4 emissions across the U.S. were ~1.7 and ~1.5 times larger than the EDGAR4.2 and U.S. EPA national inventories. They attributed the bias to oil/gas and livestock emissions, but they were unable to quantitatively separate the two, owing to their spatial overlap and limited observational coverage.

Wetland emissions remain one of the key sources of uncertainty in the regional to global atmospheric CH_4 budget, largely due to poor understanding of the biophysical processes controlling production and consumption in saturated soils (Bloom et al., 2017; Nisbet et al., 2014). Within the U.S. Corn Belt, Zhang, Lee, Griffis, Baker, and Xiao (2014) used tall tower measurements to infer a CH_4 budget that was 5.8 times greater than EDGAR42 and hypothesized that the difference could be attributed to wetland emissions. A geostatistical inverse modeling study of Miller et al. (2014) indicated a large emission underestimate by the existing inventory (e.g., Kaplan model; Kaplan, 2002) for Minnesota and Wisconsin wetlands. Recent inverse modeling studies using satellite observations also support major wetland CH_4 emissions for Florida as well as the Midwest (Turner et al., 2015; Wecht et al., 2014).

At finer spatial scales within the region, recent studies have quantified CH_4 fluxes from wetlands, agricultural crops, and livestock facilities. Olson et al. (2013) found that CH_4 emissions from a temperate peatland in north-central Minnesota showed instantaneous fluxes reaching a maximum of 290 nmol m^{-2} s^{-1} in August, with an annual budget ranging from 15.7 to 33.2 g CH_4 m^{-2} yr^{-1} over the period 2009 to 2011. The instantaneous fluxes and annual budget were very sensitive to peat temperature and water table position. In contrast, CH_4 fluxes from individual corn and soybean plants were extremely small, ranging from about +0.4 nmol m^{-2} s^{-1} during the day to about −0.8 nmol m^{-2} s^{-1} during the night (Zhang, Lee, Griffis, Baker, Erickson, et al., 2014). Bavin et al. (2009) also showed that soil CH_4 fluxes from conventional and reduced tillage corn-soybean rotations were most often below the flux detection limit of static chambers.

There is a paucity of studies that have examined enteric CH_4 emissions and emissions related to manure management from within the region. Methane emissions have been reported for dairy manure storage facilities in Wisconsin (a simple storage basin) and Indiana (a storage lagoon, in which solids had previously been removed) (Grant et al., 2015). On a per animal basis, CH_4 emissions were larger from the storage basin than the lagoon with mean daily emissions of 295 g CH_4 $head^{-1}$ d^{-1} (374 g AU^{-1} d^{-1}) and 47 g CH_4 $head^{-1}$ d^{-1} (59 g AU^{-1} d^{-1}), respectively (AU represents Animal Unit, where 1 AU = 500 kg live weight). These daily emissions were shown to follow a positive linear relation with temperature. The relative lower emissions from the lagoon storage facility were attributed to the lower availability of carbon due to removal of solids prior to storage. The area-based flux estimates were 94 kg CH_4 m^{-2} yr^{-1} and 80 kg CH_4 $m^{-2}yr^{-1}$, respectively, and were estimated to be less than the enteric emissions from these farms (Grant et al., 2015).

Enteric emissions from dairy cows can show substantial variability depending on size, sex, growth stage, activity (i.e., lactating versus dry), and diet (Lassey, 2007). Because of limited studies conducted for the U.S. Midwest, we draw on some recent studies from outside of the region. On-farm flux estimates, based on a backward Lagrangian stochastic technique, showed that enteric emissions ranged from 270 to 380 g (lactating cow d)$^{-1}$ for two dairy farms in Ontario, Canada, and accounted for about 40% of the total CH_4 farm emissions (Vanderzaag et al., 2014). Recent studies have shown that enteric emissions from dairy cows can be significantly reduced by using inhibitors designed to improve carbon use efficiency. Hristov et al. (2015) showed that enteric emissions varied from 400 to 500 g CH_4 d^{-1} and 290 to 390 g CH_4 d^{-1} over a 12 week period without/with the use of an inhibitor (3NOP), respectively.

Here we build on our previous work (Olson et al., 2013; Zhang, Lee, Griffis, Baker, Erickson, et al., 2014; Zhang, Lee, Griffis, Baker, & Xiao, 2014) and use tall tower aerodynamic flux measurements and SFBI analyses to obtain improved constraints on the CH_4 emissions from natural and anthropogenic sources within the region. The objectives were to (1) estimate the regional CH_4 budget, (2) partition the emissions into natural and anthropogenic sources, and (3) identify sources and time periods associated with high CH_4 emissions to improve our understanding of potential mitigation options.
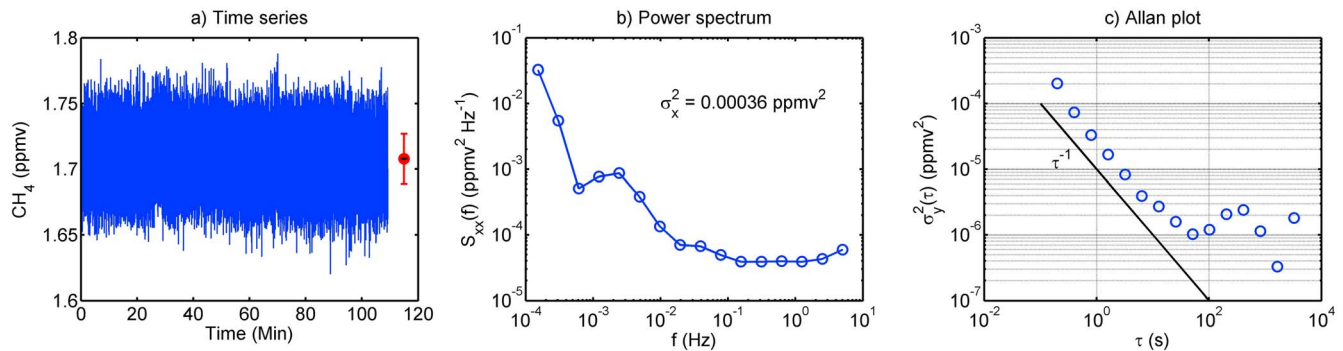
Figure 1. Results of sampling a standard gas cylinder including (a) the 10 Hz time series with the mean ± 1 SD (red symbols/bars) and mean ± 1 SE (black), (b) the power spectrum of the concentration series (as spectral densities), and (c) an Allan variance plot.

2. Methods

2.1. Study Site

The University of Minnesota tall tower trace gas observatory (KCMP tall tower; 244 m height) is located 25 km south of the Saint Paul-Minneapolis Metropolitan area in the Midwestern United States. The landscape is highly heterogeneous with agricultural lands predominant to the east, south, and west. To the north and northwest, there is a strong gradient from agricultural land to a relatively dense urban landscape. Detailed land use statistics as a function of distance and direction from the tall tower study site have been reported previously (Chen et al., 2016; Griffis et al., 2013). The study domain contains 10 states in the U.S. Midwest including Minnesota, Illinois, Indiana, Iowa, Missouri, Ohio, North Dakota, South Dakota, Nebraska, and Wisconsin.

2.2. Methane Mixing Ratio Observations

The KCMP tall tower has been instrumented with meteorological and trace gas sensors since April 2007. Carbon dioxide, water vapor, and nitrous oxide have been measured at sample heights of 32, 56, 100, and 185 m (Griffis et al., 2013, 2017; Zhang, Lee, Griffis, Baker, & Xiao, 2014). Turbulence is measured at 100 and 185 m using sonic-anemometers (model CSAT3; Campbell Scientific Inc., Logan, Utah). Near-continuous measurement of CH_4 mixing ratios was initiated in May 2016 using a Trace Gas Analyzer (TGA200A, Campbell Scientific Inc., Logan, Utah, USA). This system uses a state-of-the-art interband cascade laser that is thermoelectrically cooled to a temperature of 17 °C. The manufacturer's reported measurement noise, based on the Allan variance, is 7.0 nmol mol^{-1} for an integration period of 100 ms. Our field tests indicated that the noise is approximately 9.5 nmol mol^{-1} for an integration period of 60 min (Figure 1). As shown later, this measurement noise is extremely small compared to the temporal fluctuations in the tall tower observations. The TGA is calibrated hourly against an ultrapure zero air standard and a working CH_4 span gas that was propagated from our Earth System Research Laboratory (National Oceanic and Atmospheric Administration [NOAA] Earth System Research Laboratory) gold standard (Cylinder ID: CB11952, mole fraction = 1,849.9 nmol mol^{-1}, reproducibility = 1 nmol mol^{-1}, WMO-CH$_4$-X2004A Calibration scale). Sample air is pulled continuously from inlets at 185 and 3 m at a total flow rate of approximately 15 SLPM at approximately 50 kPa. The 185 and 3 m sample inlets are subsampled at 30 s intervals. The air samples are dehumidified using a Nafion dryer system prior to analysis.

2.3. Flux-Gradient Method

The CH_4 mixing ratio gradients and fluxes provide information related to the landscape (i.e., mesoscale; approximately hundreds of km^2) footprint, while the SFBI analyses constrain sinks and sources at the regional scale (approximately thousands of km^2) (Zhang, Lee, Griffis, Baker, & Xiao, 2014).

The aerodynamic flux was estimated from

$$F_C = -K_C m_a \frac{dC}{dz} + F_s \tag{1}$$

where the eddy diffusivity (K_C) was estimated from the momentum flux measured using eddy covariance at a
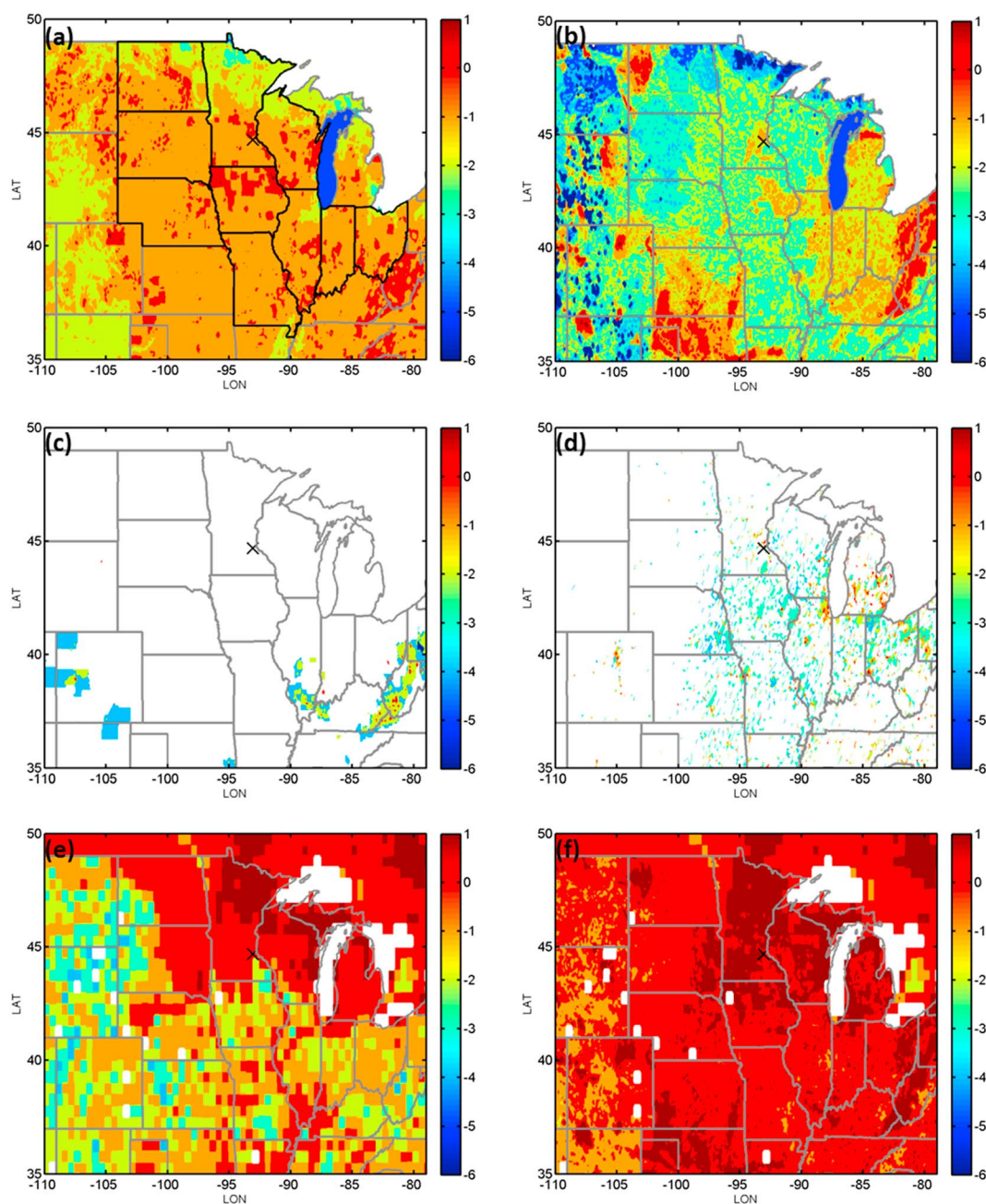
Figure 2. The a priori annual average emissions from (a) livestock, (b) natural gas + oil, (c) coal mining, (d) waste, (e) natural wetlands, and (f) total (unit is $\log_{10}(\text{nmol m}^{-2}\text{ s}^{-1})$). Anthropogenic source categories including livestock, oil/gas, coal mining, and waste were from Maasakkers et al. (2016), and the natural wetland emissions were derived from Bloom et al. (2017). The KCMP tall tower is indicated by the black crosses in each panel.

height of 185 m (Wood et al., 2016), m_a is the molar density of dry air, dC/dz is the CH_4 mixing ratio gradient, and F_s is an estimate of the change in hourly CH_4 storage integrated over a height of 185 m. An enhancement factor of 1.35 was applied to K_c to account for the difference between momentum and a trace gas scalar diffusivity (Simpson et al., 1998).

2.4. Inverse Modeling Framework

Here we apply a Bayesian inversion to interpret the tall tower observations in terms of a constraint on the regional CH_4 sources in the U.S. Midwest. The Stochastic Time-Inverted Lagrangian Transport (STILT) model (Gerbig et al., 2003; Lin et al., 2003, 2004) was used to estimate the tall tower concentration source

Table 1
Sites of Flask CH$_4$ Observations Used in This Study

NOAA code	Location	Country	Latitude	Longitude
AMT	Argyle, Maine	United States	45.035	−68.682
DND	Dahlen, North Dakota	United States	47.5	−99.24
ESP	Estevan Point, British Columbia	Canada	49.383	−126.544
ETL	East Trout Lake, Saskatchewan	Canada	54.35	−104.983
HIL	Homer, Illinois	United States	40.07	−87.91
LEF	Park Falls, Wisconsin	United States	45.945	−90.273
MWO	Mt. Wilson Observatory	United States	34.225	−118.059
NWR	Niwot Ridge, Colorado	United States	40.053	−105.586
SGP	Southern Great Plains, Oklahoma	United States	36.607	−97.489
THD	Trinidad Head, California	United States	41.054	−124.151
UTA	Wendover, Utah	United States	39.902	−113.718
WBI	West Branch, Iowa	United States	41.725	−91.353
WGC	Walnut Grove, California	United States	38.265	−121.491

footprint using the sample inlet (receptor) at a height of 185 m and atmospheric drivers (e.g., planetary boundary layer [PBL] height, wind, and atmospheric stability) obtained from the Weather Research and Forecasting (WRF) model version 3.8.1 (Nehrkorn et al., 2010). The source footprint was then multiplied by a bottom-up emission inventory (a priori sources) and combined with the background mixing ratios to provide an initial estimate of the hourly CH$_4$ mixing ratios at the tall tower receptor (Figure 2).

2.4.1. Prior Information

The Bayesian inverse analysis relies heavily on the prior spatial distribution of associated source categories, and it is therefore critical to use emission inventory data that have high spatial accuracy for proper attribution. EDGAR42 is one of the most comprehensive bottom-up inventories but has been reported to show poor spatial accuracy in regional CH$_4$ emissions, particularly from the livestock and oil/gas sectors (Miller et al., 2013; Turner et al., 2015; Wecht et al., 2014). In EDGAR42, the oil/gas emissions are too heavily weighted by the spatial distribution and usage rather than the production (Miller et al., 2013; Maasakkers et al., 2016). Further, the oil/gas sector has a strong correlation ($R^2 > 0.8$) with waste emissions because both are largely distributed according to human population. Therefore, a Bayesian inversion using EDGAR42 as the a priori estimate could wrongly attribute sources (e.g., assign CH$_4$ emissions from oil/gas production sites to livestock). For these reasons, we decided to use the gridded EPA inventory (Maasakkers et al., 2016) to represent the a priori anthropogenic sources.

The EPA inventory is available only as national totals for different source types (EPA, 2016). Maasakkers et al. (2016) used a range of databases at the state to local source levels to disaggregate the inventory and allocated the spatial distribution of emissions for individual source types and presented a gridded inventory of U.S. anthropogenic CH$_4$ emissions with 0.1° × 0.1° spatial resolution and detailed scale-dependent error characterization. Their estimate showed a significant spatial difference compared with EDGAR42, particularly for oil/gas systems and manure management. The gridded EPA inventory for the year 2012 placed higher emissions over oil/gas production areas and lower emissions over distribution areas, consistent with recent top-down constraints across the U.S. (Miller et al., 2013; Turner et al., 2015).

Initially, (1) enteric fermentation, (2) manure management, (3) natural gas, (4) oil, (5) coal mining, (6) waste, (7) natural wetlands, and (8) others (i.e., forest fire hotspots and stationary combustion emissions) were adopted here as a priori source categories. However, spatially overlapping characteristics of enteric fermentation and manure management, as well as natural gas and oil, respectively, placed strong limitations on identifying and separating them individually within the inversion framework (Turner & Jacob, 2015). Therefore, we combined enteric fermentation and manure management as livestock and combined natural gas and oil as gas/oil. Furthermore, Bloom et al. (2017) provided a full (2009–2010) and extended (2001–2015) estimate of wetland emissions, based on knowledge of regional to global wetland CH$_4$ sources and its biophysical controls. We adopted the full estimate of wetland emissions with a gridded resolution of 0.1° × 0.1°, which was developed based on satellite-derived surface water content and precipitation reanalyses, as well as environmental parameterizations.

Other sources such as forest fire hotspots and stationary combustion were insignificant for the Midwest and not feasible to independently constrain from atmospheric data. Therefore, these sources were not included in
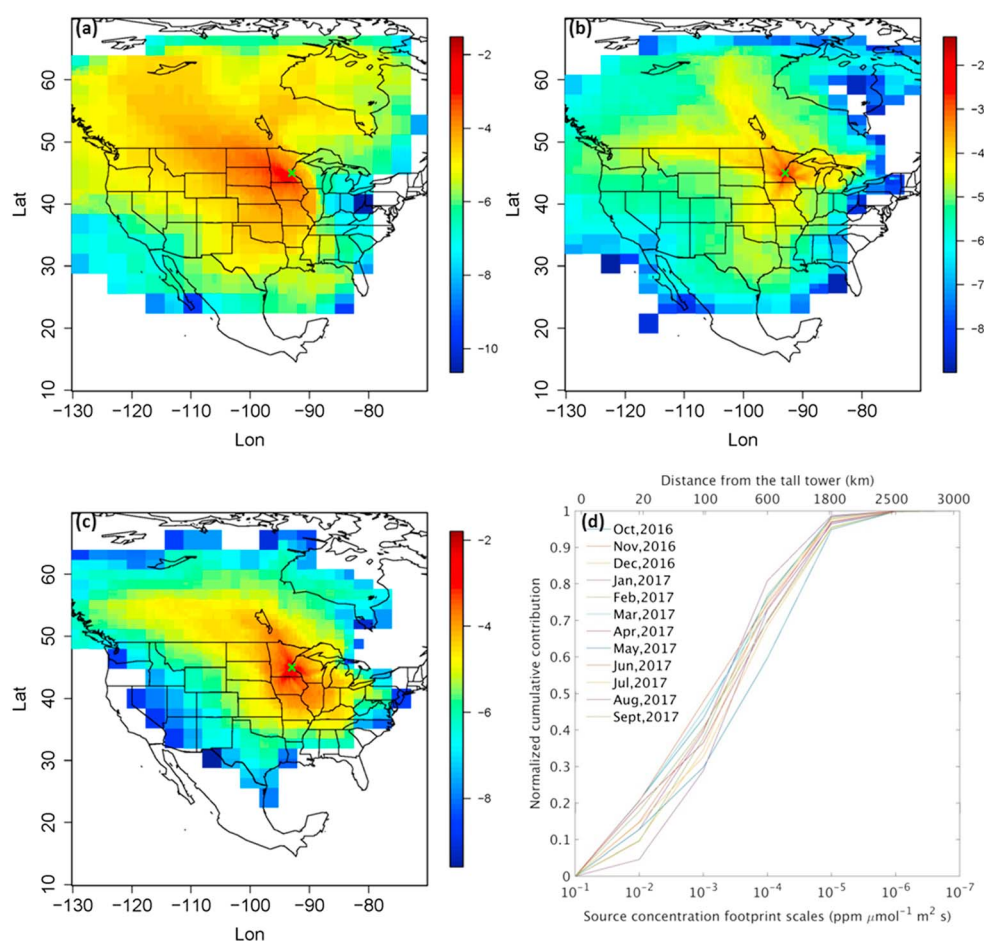
Figure 3. Source footprint functions (units: $\log_{10}$(ppm µmol^{-1} m^2 s)) for measurements at the KCMP tall tower (indicated by crosses). (a) December 2016; (b) March 2017; (c) August 2017. (d) Normalized cumulative contribution as a function of source footprint scale (ppm µmol^{-1} m^2 s) and the corresponding distance from the tall tower (km).

the a priori estimate. The five source categories included in the a priori emission inventory were the following (Bloom et al., 2017; Maasakkers et al., 2016): (1) livestock, including enteric fermentation and manure management; (2) gas/oil, including natural gas production, processing, transmission, and distribution, as well as petrochemical production; (3) waste, including landfills and wastewater treatment; (4) coal mining, both surface and underground; and (5) monthly natural wetlands and peatlands from Bloom et al. (2017).

We define the a priori errors for livestock, gas/oil, waste, and coal mining sources at 0.1° × 0.1° resolution based on the corresponding scale-dependent errors developed by Maasakkers et al. (2016) for the gridded EPA inventory. Bloom et al. (2017) derived 324 ensemble models of wetland CH_4 emissions in 2009 and 2010, based on 3 CH_4: C temperature dependencies (i.e., the temperature dependence of the ratio of C respired as CH_4), 9 heterotrophic respiration configurations, 4 wetland extent scenarios, and 3 global scaling factor (i.e., a global budget estimate from wetland emissions) configurations. Here we used the ensemble mean of 324 model realizations for the year 2010 as the a priori estimate, and its coefficient of variation as the associated a priori error. Based on the derived a priori errors (i.e., 79–95%) we rounded them to 100% for each source category.

2.5. Concentration Footprint Functions

Concentration source footprint functions were determined based on the STILT model. For each hour between June 2016 and September 2017, we released 500 particles from the KCMP tall tower at a height of 185 m and transported them backward for 7 days to ensure that the trajectories adequately represented source contributions from within the U.S. Furthermore, we used observations (Table 1) from the NOAA Carbon Cycle and
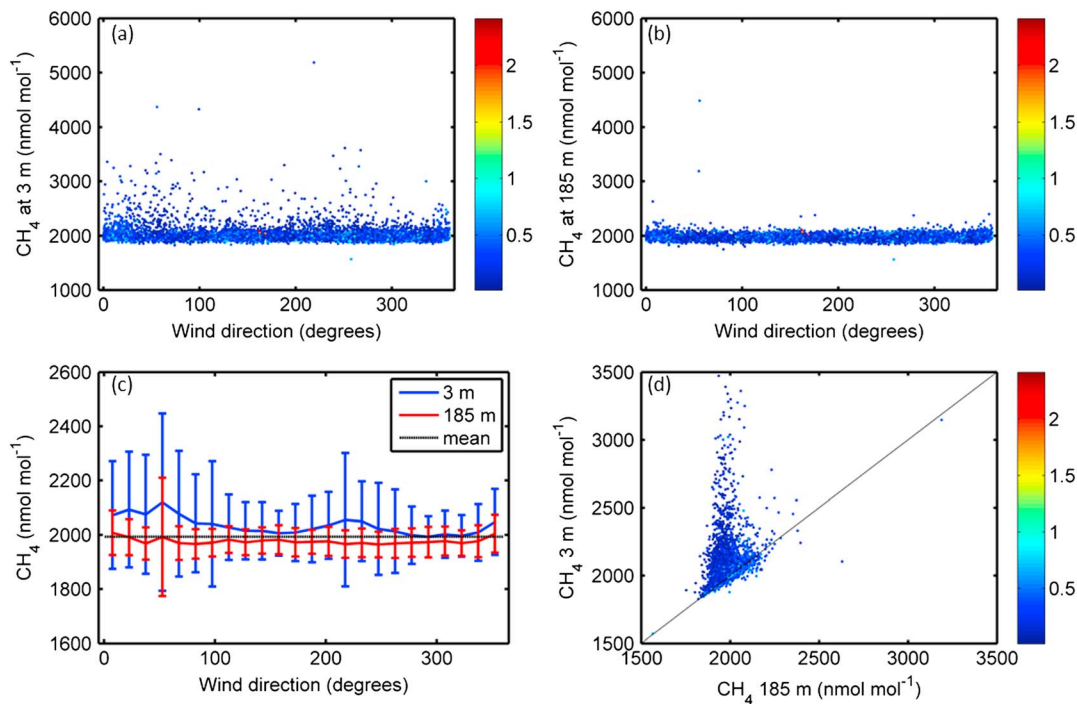
Figure 4. Hourly mean CH_4 mixing ratios measured at (a) 3 m and (b) 185 m as a function of wind direction. The color bar represents the friction velocity value (m s^{-1}). (c) Mean methane mixing ratios (±1 standard deviation) as a function of wind direction binned using 15 degree intervals. (d) Relation between CH_4 mixing ratios measured at 3 m versus 185 m. The color bar indicates the friction velocity value. Each data point represents an hourly average value. Note that the 1:1 line is obscured by the best fit linear regression line.

Greenhouse Gases program near the outer edge of the source footprint to represent the background CH_4 mixing ratios. These observations are from discrete air samples collected approximately weekly in flasks (Dlugokencky et al., 2009, 2011) and are zonally and monthly averaged at 4° latitudinal resolution.
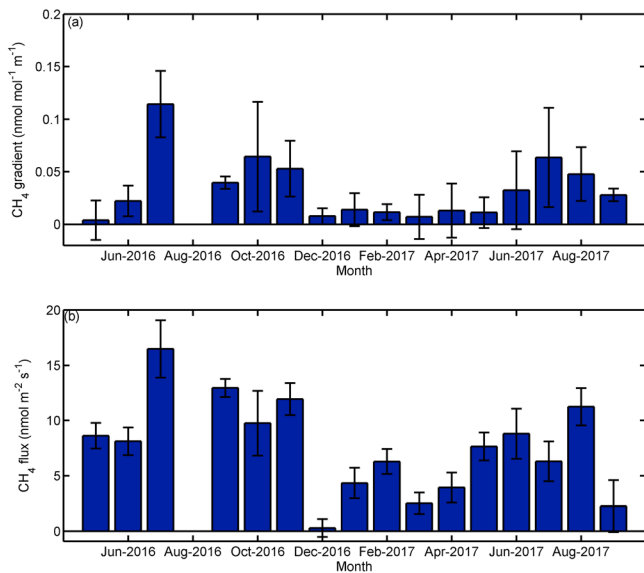
Examples of the concentration footprint functions during years 2016 and 2017 at the tall tower are shown in Figures 3a–3c. For each month, based on the a priori inventory, we calculated the cumulative contribution of surface emissions to the tall tower mixing ratio at a range of concentration footprint scales and the corresponding distance from the tall tower (Figure 3d). These analyses indicated that areas where the footprint strength was greater than 1e − 4 ppm μmol^{-1} m^2 s contributed significantly to the tall tower mixing ratios (i.e., they accounted for about 75% of the total contribution). These intense areas contain Minnesota and a significant portion of the U.S. Midwest. The tall tower observations, therefore, are representative of the larger Midwest region (Griffis et al., 2013; Zhang, Lee, Griffis, Baker, & Xiao, 2014) and should provide a reasonably robust estimate of CH_4 emissions and their partitioning via the SFBI approach.

2.6. Methane Budget and Partitioning

Here we used the SFBI method to constrain the regional budget and to partition it into its source contributions (Chen et al., 2016; Kim et al., 2013). The SFBI method was applied monthly from June 2016 to September 2017,

Figure 5. (a) Median monthly vertical CH_4 mixing ratio gradient and (b) median monthly flux-gradient estimate. The error bars represent the standard error. Note that August 2016 is not reported due to a large fraction of missing hourly observations.
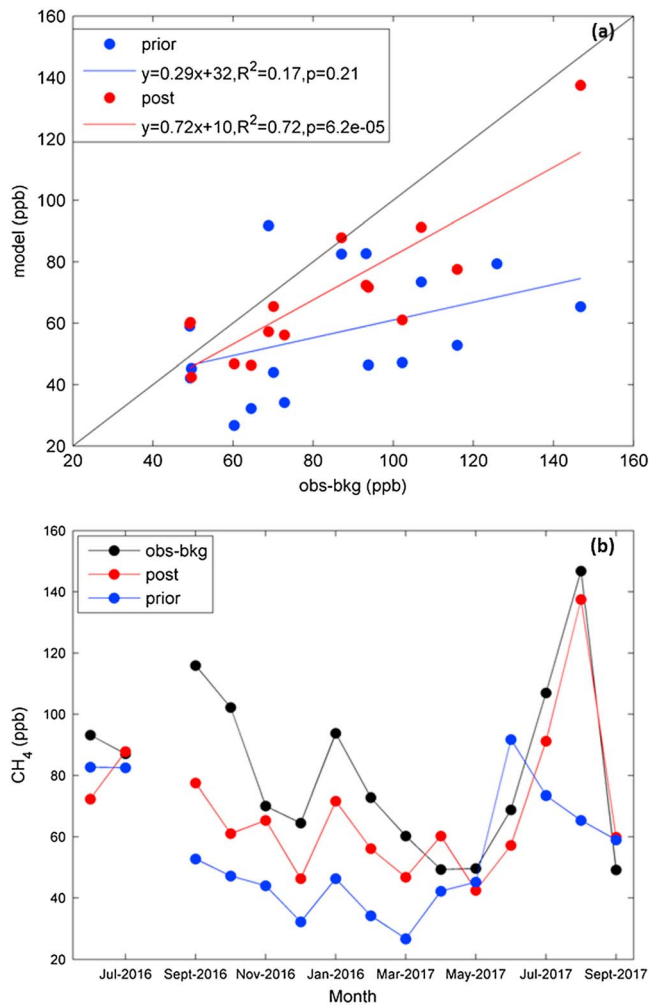
Figure 6. (a) Monthly linear regression between the observed and simulated CH_4 mixing ratios for a priori and a posteriori simulations between June 2016 and September 2017 (uncertainty values indicate a 95% confidence interval); (b) a priori, a posteriori estimate and the tall tower observations of CH_4 mixing ratios.

$$\mathbf{y} = \mathbf{K\Gamma} + \boldsymbol{\varepsilon} \qquad (2)$$

where $\mathbf{y}$ is the mixing ratio observed at the tall tower minus the background mixing ratios, $\mathbf{\Gamma}$ contains the scaling factors for different source types, $\mathbf{K}$ is the Jacobian matrix representing the sensitivity of the observation variables to the specific source types, and $\boldsymbol{\varepsilon}$ is the system error, which consists of measurement uncertainties and model uncertainties. The columns of $\mathbf{K}$ correspond to the mixing ratios for each of the source types being optimized, and $\mathbf{\Gamma}$ consists of the a posteriori scale factors for the different source types.

Applying Bayes' theorem, along with a normal distribution assumption, the maximum a posteriori solution of $\mathbf{\Gamma}$ is to minimize the cost function $\mathbf{J(\Gamma)}$:

$$2\mathbf{J(\Gamma)} = (\mathbf{y} - \mathbf{K\Gamma})^{\mathbf{T}}\mathbf{S_\varepsilon}^{-1}(\mathbf{y} - \mathbf{K\Gamma}) + (\mathbf{\Gamma} - \mathbf{\Gamma_a})^{\mathbf{T}}\mathbf{S_a}^{-1}(\mathbf{\Gamma} - \mathbf{\Gamma_a}) \qquad (3)$$

where S_ε and S_a are the observational and a priori error covariance matrices, and each element of $\mathbf{\Gamma_a}$ = 1. The solution to $\nabla\mathbf{\Gamma J(\Gamma)} = 0$ is then given by:

$$\mathbf{\Gamma_{post}} = \left(\mathbf{K^T S_\varepsilon}^{-1}\mathbf{K} + \mathbf{S_a}^{-1}\right)^{-1}\left(\mathbf{K^T S_\varepsilon}^{-1}\mathbf{y} + \mathbf{S_a}^{-1}\mathbf{\Gamma_a}\right) \qquad (4)$$

Here observational errors include measurement and modeling uncertainties. The mixing ratio measurement error for the TDL was based on the Allan variance test described above (9.5 nmol mol^{-1} for an integration period of 60 min). Further, Gerbig et al. (2003) conducted a wide range of sensitivity tests by varying the released number of particles from 50 to 1,000 in the STILT model, and each test was run 100 times to analyze the particle number dependence and reproducibility. Following the work of Gerbig et al. (2003), a relative uncertainty of 13% was assigned for the number of particles used in the backward trajectories. In this study, the transport error associated with the number of particles used ranged from ~6 to 9 ppb. We used different PBL schemes, that is, Yonsei University (Hong et al., 2004) and Mellor-Yamada-Janjic (Janjic, 2002), to simulate the mixing height from the WRF-STILT simulations. The modeled mixing heights were then compared to that inferred from the radiosonde observations (Kim et al., 2013; Miller et al., 2008) to derive the relative uncertainty associated with the simulated PBL height, which was estimated to be 27%. The transport error associated with the PBL height simulations ranged from ~10 to 16 ppb. Finally, it is critical to use mass conserving wind fields to drive the transport (Gerbig et al., 2003). The WRF simulations used in this study are constructed specifically for mass conservation and have been found to perform better than other meteorological products (Miller et al., 2013; Nehrkorn et al., 2010). A detailed uncertainty analysis associated with aggregation error is presented in section 3.

3. Results and Discussion

3.1. Methane Mixing Ratios and Fluxes

Mean CH_4 mixing ratios at 3 and 185 m (1 June 2016 to 30 September 2017) were 2,024.4 ± 132.4 nmol mol^{-1} and 1,982.0 ± 54.4 nmol mol^{-1}, respectively (Figure 4). Wind direction had a relatively weak influence on the CH_4 mixing ratios at 3 m (Figure 4). For example, advection from the urban airshed to the north resulted in CH_4 mixing ratios that were about 100 nmol mol^{-1} higher than the ensemble mean mixing ratio. There is also a small but noticeable increase in CH_4 mixing ratio from the southwest wind sector, which is predominantly agricultural land use. Hourly CH_4 mixing ratios at the 185 and 3 m levels were highly correlated ($r^2 = 0.976$, $n = 5,305$, $p < 0.0001$). The large deviations from the 1:1 line (Figure 4d) were generally associated with weak turbulent mixing (i.e., when friction velocity was less than 0.1 m s^{-1}).

Table 2
Annual Mean A Priori and A Posteriori Emissions and Scaling Factors for Each Source Category (from October 2016 to September 2017)

Emissions (Tg CH_4 yr^{-1})	Wetlands	Livestock	Oil/gas	Waste	Total	Anthropogenic
A priori	3.8	2.6	1.2	1.3	8.9	5.1
A posteriori	4.0 ± 1.2	4.8 ± 1.5	1.6 ± 0.6	1.4 ± 0.6	11.8 ± 2.0	7.8 ± 1.6
Scale factor	1.1	1.8	1.3	1.1	1.3	1.5

Vertical CH_4 gradients were very small in the winter (December through March) compared to the midsummer (July through August, Figure 5a), indicating that within the aerodynamic flux footprint, microbial activity was the main driver of emissions (i.e., not fuel production or consumption). Further, there was a relatively low frequency of negative mixing ratio gradients, implying that the agricultural landscape was rarely a net CH_4 sink.

The mean aerodynamic CH_4 flux was +13.7 ± 0.34 (mean ± standard error) nmol m^{-2} s^{-1} (Figure 5), which equates to a net CH_4 source of about 6.9 g CH_4 m^{-2} yr^{-1}, and is in good agreement with previous estimates at the landscape scale (Zhang, Lee, Griffis, Baker, Erickson, et al., 2014).

3.2. Bayesian Analyses

After the first inversion, the averaging kernel (AK) was calculated to quantify the sensitivity of retrieved emissions to their true values (Chen et al., 2016; Kim et al., 2013; Rodgers, 2000). The AK values indicated a very low sensitivity of tall tower observations to the coal mining source, probably due to the limited near-field distribution relative to the tall tower receptor (Figure 2c). Therefore, we eliminated the coal mining source term from further consideration and applied a second inversion where we only included the livestock, oil/gas, waste, and natural wetland and peatland source categories. This second inversion produced the final optimized emission estimates.

Figure 6a illustrates the linear regressions between the measured and simulated CH_4 mixing ratios based on the a priori and a posteriori estimates. The optimized CH_4 mixing ratios showed a much stronger correlation (R^2 = 0.72 and p = 6.2e-5) than the a priori estimate (R^2 = 0.17 and p = 0.21), and the slope increased from 0.29 ± 0.17 to 0.72 ± 0.12, indicating that the optimization helped to reduce the model bias and significantly improved the constraint on the emissions (Figure 6 b). Based on the cost function analysis (equation (3)), the optimization is constrained to a certain degree by the error construction of observations and the a priori estimate; for example, decreasing the observational errors or increasing the a priori errors leads to an increase in the optimized scaling factors and acted to increase the slope of the linear regression between the modeled and observed CH_4 mixing ratios. A detailed analysis of the improvement of the inverse model performance is provided in section 3.4.

From the second inversion, there was a mean scaling factor of 1.5 relative to the gridded EPA inventory for anthropogenic sources (Table 2). Among them, optimized livestock and oil/gas sources were 1.8 and 1.4 times greater (Figure 7a), respectively, in close agreement with other recent studies (Miller et al., 2013; Turner et al., 2015). The optimized mean annual anthropogenic CH_4 emission was 12.3 ± 2.1 nmol m^{-2} s^{-1} for the Midwest region. Compared to the source attribution for the national-scale budget, there was a higher contribution from livestock and lower contribution from oil/gas sources for the U.S. Midwest, corresponding to its agriculture-dominated land use characteristics.

Wetlands within our study domain are largely distributed in central and northern Minnesota as well as Wisconsin (Cohen et al., 2016), among the

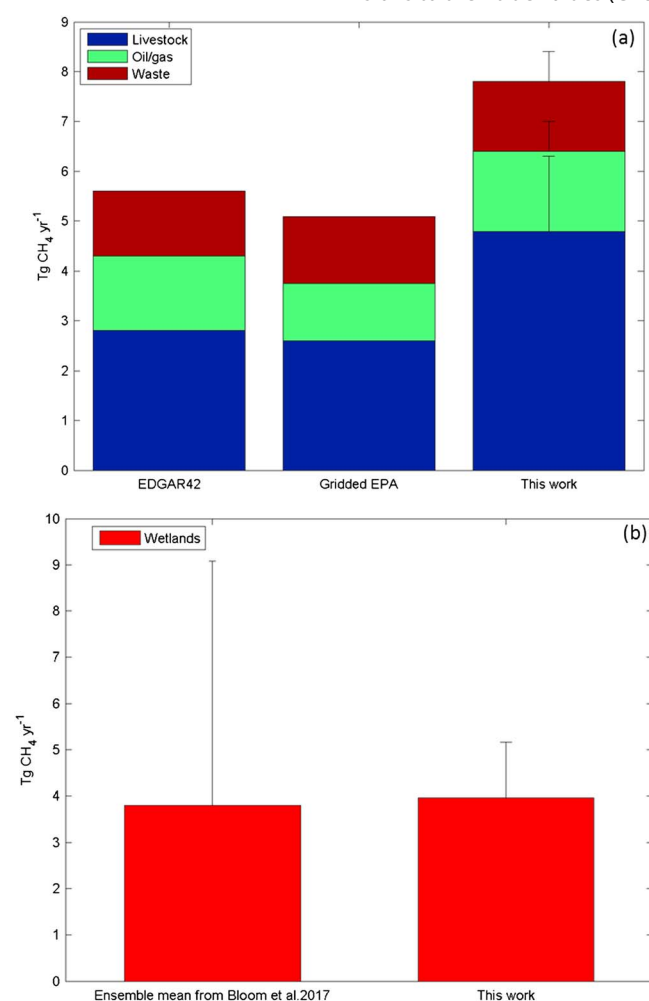**Figure 7.** Annual regional CH_4 emissions within the U.S. Midwest from different studies including (a) anthropogenic and (b) natural sources. The error bars indicate the uncertainties of the regional emission estimate from each source, respectively.
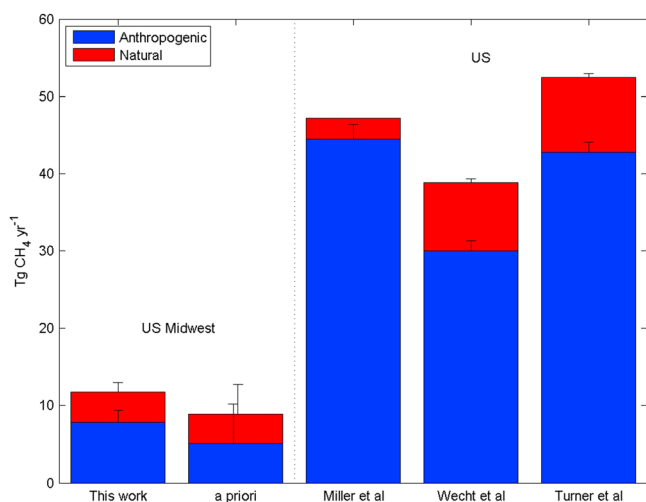
Figure 8. Regional and national methane budgets for natural and anthropogenic sources. The error bars indicate the uncertainties of the regional emission estimate from anthropogenic and natural sources, respectively.

most sensitive areas to the tall tower receptor based on the concentration footprint functions (Figure 3). The optimized wetland emissions are in excellent agreement with the estimate from Bloom et al. (2017) (Figure 7b) and represent the second largest source (4.0 Tg CH_4 yr^{-1}), accounting for 34% of total CH_4 emissions within the Midwest region (Table 2).

Compared to the CH_4 emission estimate at the national scale from the most recent space-based study (Turner et al., 2015), our work suggests that the natural, anthropogenic, and total CH_4 emissions in the Midwest account for 41.7 ± 12.5%, 18.2 ± 3.7%, and 22.5 ± 3.8% of the U.S. budget, respectively (Figure 8). This further supports the importance of the U.S. Midwest to the national and global CH_4 budget and highlights the need to understand how these emissions are likely to respond to changes in land management and climate.

3.3. Seasonality Analysis

The temporal variability of total optimized CH_4 emissions was dominated by wetlands (Figure 9). Since emissions from oil/gas, livestock, and waste showed relatively weak seasonality, the contribution from wetland emissions well explained the seasonal variation of the tall tower CH_4 mixing ratios. The wetland emissions were very weak from November to February, began to rise after snowmelt in March, and peaked in August. This seasonality agrees closely with eddy covariance observations and retrospective modeling studies at Bog Lake Fen, Marcell Experiment Forest Station in northern Minnesota (Olson et al., 2013).

To further explore the climate sensitivity of the regional methane emissions, the weighted means of selected environmental variables from the National American Regional Reanalysis (Mesinger et al., 2006) data were computed for the entire study domain. Here the weighting is based on the intensity of the source footprint function for each grid cell. The seasonal and interannual variations of optimized wetland emissions appear to be consistent with variations in air temperature. We found that the peak CH_4 emissions in August were coincident with maximum source footprint-weighted soil temperature, which also agreed with earlier observations at the Marcell Experiment Forest Station, where CH_4 emissions peaked with peat temperature (Olson et al., 2013). Olson et al. (2013) reported increased CH_4 emissions at Bog Lake Fen in warm years including 1994, 2001, and 2005 and suggested that temperature dominated the temporal variability, while water table depth played a lesser role.
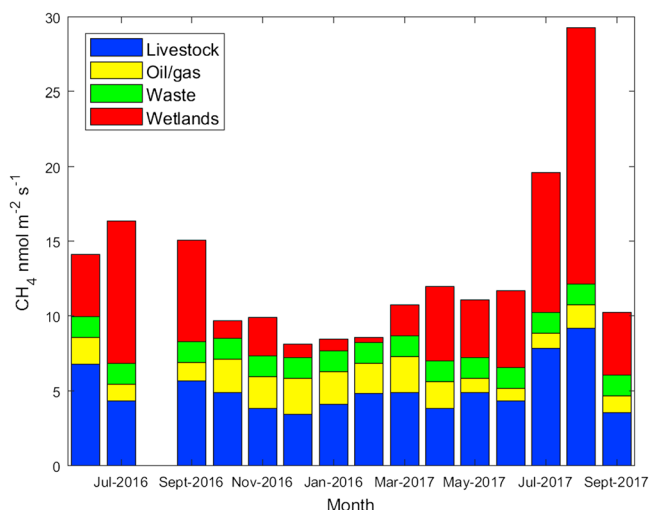
The notably higher temperature (1.5 °C within the growing season) in 2016 compared to 2017 likely enhanced wetland emissions. For instance, the weighted September air temperature was 2.3 °C higher in 2016, and the corresponding regional wetland emissions were 62% higher compared to 2017. Conversely, there appears to be very limited impact of precipitation differences on the wetland emissions. For example, June 2016 and September 2017 experienced dramatically different precipitation amounts (106.0 versus 24.7 mm, respectively), yet the regional wetland emissions (4.16 versus 4.22 nmo m^{-2} s^{-1}) were not statistically different.

Finally, it is possible that the warmer conditions stimulated higher CH_4 emissions from manure. For instance, the June and September air temperatures were 1.1 and 2.3 °C higher in 2016, and the corresponding regional livestock emissions were 56% and 60% higher than in 2017. Since enteric emissions are less dependent on air temperature (i.e., animal body temperature is regulated), stronger air temperature sensitivity for manure emissions is expected (Dong et al., 2006; Sommer et al., 2004; Wood et al., 2013).

Figure 9. Optimized monthly variation of CH_4 emissions for each source category, including the livestock, oil/gas, waste, and wetlands.

Table 3
The A Posteriori Emissions With Various Sensitivity Tests on Background Mixing Ratios

Background mixing ratios	A posteriori emissions (Tg CH$_4$ yr^{-1})					
	Wetlands	Livestock	Oil/gas	Waste	Total	Anthropogenic
Mean − 2 SD	4.5	5.4	1.7	1.5	13.1	8.6
mean − 1 SD	4.3	5.3	1.6	1.2	12.4	8.1
Mean	4.0	4.8	1.6	1.4	11.8	7.8
mean + 1 SD	3.6	4.5	1.6	1.4	11.1	7.5
mean + 2 SD	3.3	4.2	1.4	1.4	10.3	7.0

3.4. Uncertainty Analysis

To probe how aggregation error influenced the Bayesian inversion, we decreased the spatial resolution of the a priori emissions and meteorological fields from 0.1° × 0.1° to 0.5° × 0.5° for each source category. We then reran STILT to obtain the source footprint functions at 0.5° × 0.5° resolution and applied the SFBI in an otherwise identical fashion to our previously described approach. The low-resolution inversion showed that when decreasing the resolution: (1) the correlation among source categories became stronger, for example, the correlation coefficient (R) between livestock and oil/gas increased from 0.35 to 0.56, and (2) the scale factor for the livestock source increased while that for the oil/gas source decreased. Further, we found that the AK for oil/gas source decreased from 0.89 to 0.55, indicating a weak sensitivity to the tall tower observations. As expected, averaging the inventory over a coarser grid caused spatial overlapping among source categories, leading to higher correlation among them. Using a priori information with a coarser resolution reduces the amount of independent information contained in the a priori inventory. The source(s) of interest cannot be separated and results in a lower sensitivity to the tall tower observations, providing a weak constraint within the inverse modeling framework.

Further, we examined the potential impact of having an upward/downward bias in the background CH$_4$ concentrations on the Bayesian inversion. Here we conducted a range of sensitivity tests by varying the monthly background mixing ratios (from mean − 2 SD to mean + 2 SD) based on the discrete flask-air observations from the NOAA Carbon Cycle and Greenhouse Gases program. These sensitivity analyses revealed that the annual budget ranged from 10.3 to 12.4 Tg CH$_4$ yr^{-1}, which showed only a minor variation (5%–12%) compared to the best estimate (Table 3). These analyses suggest that the optimized annual budget and the source attribution show low sensitivity to the uncertainties in the background mixing ratios, and support that background CH$_4$ values are reasonably constructed and provide a reliable estimate for the Bayesian inversion framework.

Finally, by assembling key parameterizations in the models from Bloom et al. (2017), a range of a priori wetland emission scenarios were applied for the sensitivity tests (Table 4), to assess how well the inversion constrained the wetland source. The sensitivity studies showed similar seasonality and an annual wetland

Table 4
Wetland CH$_4$ Model Ensemble Configurations

Tests	Global scale factor (Tg CH4 yr^{-1})	CH$_4$: C temperature dependence (Q_{10})	Heterotrophic respiration	Wetland extent scenario	Wetland emissions (Tg CH$_4$ yr^{-1})
S1	124.5	1.0	Ensemble mean from the multiscale Synthesis and Terrestrial Model Intercomparison Project (MsTMIP)[a,b]	GLOBCOVER spatial extent[c] and SWAMPS[c] inundation temporal variability parameterization	3.76
S2	124.5	2.0			3.74
S3	124.5	3.0			3.54
S4	166.0	1.0			3.63
S5	166.0	2.0			4.26
S6	166.0	3.0			3.41
S7	207.5	1.0			4.0
S8	207.5	2.0			4.38
S9	207.5	3.0			4.16

[a]Huntzinger et al. (2013).   [b]Wei et al. (2014).   [c]Schroeder et al. (2015).   [d]Bontemps et al. (2011).

budget that ranged from 3.41 to 4.38 Tg CH_4 yr^{-1} or 86.1% to 110.7% of the best estimate (4.0 Tg CH_4 yr^{-1}). This supports a relatively robust constraint of the wetland source in the Bayesian inversion.

An important question is, to what extent can we improve the CH_4 budget estimate for the U.S. Midwest? Currently, there are two critical limitations, including the spatially sparse tall tower concentration observations and the lack of direct flux measurements of key land use categories. Building on previous inverse studies (Chen et al., 2016; Griffis et al., 2017; Michalak et al., 2017; Turner et al., 2015), the following recommendations are made in order to help reduce regional scale uncertainties. There is a need for (1) improved high-resolution information on activity data to better specify the a priori source distribution, (2) improved spatial representation of atmospheric CH_4 concentrations, and (3) direct measurement of CH_4 fluxes from underrepresented and important land use categories. To address some of these concerns our ongoing research is making use of aircraft measurement campaigns to provide new insights regarding the spatial patterns of CH_4 concentrations during key times of the year. In light of the importance of enteric emissions for the region, we have planned intensive flux measurement campaigns to improve emission estimates from large representative livestock facilities within the region. Furthermore, the measurement of the stable isotopes of CH_4 at the tall tower has significant potential to help with source attribution partitioning, error reduction in the inversion, and could provide an efficient way to assess systematic biases in the atmospheric inversion methodology.

4. Conclusions

Hourly CH_4 observations from a tall tower in the Upper Midwest United States were used to constrain the CH_4 emissions from natural and anthropogenic sources for the region based on aerodynamic flux measurements and SFBI analyses. The data and analyses support the following conclusions:

1. The mean annual landscape and regional scale CH_4 emissions (13.7 ± 0.34 versus 12.3 ± 2.1 nmol m^{-2} s^{-1}) agreed reasonably well within the margin of uncertainty.
2. Regional natural, anthropogenic, and total CH_4 emissions were 4.0 ± 1.2, 7.8 ± 1.6, and 11.8 ± 2.0 Tg CH_4 yr^{-1}, accounting for 41.7 ± 12.5%, 18.2 ± 3.7%, and 22.5 ± 3.8% of the overall U.S. natural, anthropogenic, and total CH_4 budgets, respectively.
3. Wetlands were the second largest regional source, contributing 34% to the regional budget.
4. The seasonality of total CH_4 emissions was dominated by wetlands. Wetland emissions increased significantly following snowmelt and reached a maximum in August.
5. The anthropogenic source categories were 1.5 times greater than the bottom-up inventory, with livestock and oil/gas sources underestimated by 1.8-fold and 1.3-fold, respectively.

References

Bavin, T. K., Griffis, T. J., Baker, J. M., & Venterea, R. T. (2009). Impact of reduced tillage and cover cropping on the greenhouse gas budget of a maize/soybean rotation ecosystem. *Agriculture Ecosystems and Environment*, *134*(3–4), 234–242. https://doi.org/10.1016/j.agee.2009.07.005

Bloom, A., Bowman, W. K., Lee, M., Turner, J. A., Schroeder, R., Worden, R. J., et al. (2017). A global wetland methane emissions and uncertainty dataset for atmospheric chemical transport models (WetCHARTs version 1.0). *Geoscientific Model Development*, *10*(6), 2141–2156. https://doi.org/10.5194/gmd-10-2141-2017

Bontemps, S., Defourny, P., Bogaert, E. V., Arino, O., Kalogirou, V., and Perez, J. R. (2011). Globcover products description and validation report, Tech. rep., ESA, *2011*.

Bruhwiler, L. M., Basu, S., Bergamaschi, P., Bousquet, P., Dlugokencky, E., Houweling, S., et al. (2017). U.S. CH_4 emissions from oil and gas production: Have recent large increases been detected? *Journal of Geophysical Research: Atmospheres*, *122*, 4070–4083. https://doi.org/10.1002/2016JD026157

Chen, Z., Griffis, T. J., Millet, D. B., Wood, J. D., Lee, X., Baker, J. M., et al. (2016). Partitioning N_2O emissions within the US Corn Belt using an inverse modeling approach. *Global Biogeochemical Cycles*, *30*, 1192–1205. https://doi.org/10.1002/2015GB005313

Cohen, M. J., Creed, I. F., Alexander, L., Basu, N. B., Calhoun, A. J. K., Craft, C., et al. (2016). Do geographically isolated wetlands influence landscape functions? *Proceedings of the National Academy of Sciences of the United States of America*, *113*(8), 1978–1986. https://doi.org/10.1073/pnas.1512650113

Dlugokencky, E. J., Bruhwiler, L., White, J. W. C., Emmons, L. K., Novelli, P. C., Montzka, S. A., et al. (2009). Observational constraints on recent increases in the atmospheric CH_4 burden. *Geophysical Research Letters*, *36*, L18803. https://doi.org/10.1029/2009GL039780

Dlugokencky, E. J., Nisbet, E. G., Fisher, R., & Lowry, D. (2011). Global atmospheric methane: Budget, changes and dangers. *Philosophical Transactions of the Royal Society A*, *369*(1943), 2058–2072. https://doi.org/10.1098/rsta.2010.0341

Dong, H., Mangino, J., McAllister, T. A., Hatfield, J. L., Johnson, D. E., Lassey, K. R., et al. (2006). Emissions from livestock and manure management. In H. S. Eggleston, et al. (Eds.), *2006 IPCC guidelines for national greenhouse gas inventories* (Vol. 4, pp. 1–87). Japan: IGES.

EPA (2016). Inventory of US greenhouse gas emissions and sinks: 1990−2014, 2016. Retrieved from https://www.epa.gov/ghgemissions/usgreenhouse-gas-inventory-report-1990-2014

Gerbig, C., Lin, J. C., Wofsy, S. C., Daube, B. C., Andrews, A. E., Stephens, B. B., et al. (2003). Toward constraining regional-scale fluxes of CO2 with atmospheric observations over a continent: 1. Observed spatial variability from airborne platforms. *Journal of Geophysical Research*, *108*, 4756. https://doi.org/10.1029/2002JD003018

Grant, R. H., Boehm, M. T., & Bogan, B. W. (2015). Agricultural and Forest Meteorology Methane and carbon dioxide emissions from manure storage facilities at two free-stall dairies. *Agricultural and Forest Meteorology*, *213*, 102–113. https://doi.org/10.1016/j.agrformet.2015.06.008

Griffis, T. J., Chen, Z., Baker, J. M., Wood, J. D., Millet, D. B., Lee, X., et al. (2017). Nitrous oxide emissions are enhanced in a warmer and wetter world. *Proceedings of the National Academy of Sciences of the United States of America*, *114*(45), 12,081–12,085. https://doi.org/10.1073/pnas.1704552114

Griffis, T. J., Lee, X., Baker, J. M., Russelle, M. P., Zhang, X., Venterea, R., & Millet, D. B. (2013). Reconciling the differences between top-down and bottom-up estimates of nitrous oxide emissions for the U.S. Corn Belt. *Global Biogeochemical Cycles*, *27*, 746–754. https://doi.org/10.1002/gbc.20066

Hong, S.-Y., Dudhia, J., & Chen, S.-H. (2004). A revised approach to ice microphysical processes for the bulk parameterization of clouds and precipitation. *Monthly Weather Review*, *132*(1), 103–120. https://doi.org/10.1175/1520-0493(2004)132%3C0103:ARATIM%3E2.0.CO;2

Hristov, A. N., Oh, J., Giallongo, F., Frederick, T. W., Harper, M. T., Weeks, H. L., et al. (2015). An inhibitor persistently decreased enteric methane emission from dairy cows with no negative effect on milk production. *Proceedings of the National Academy of Sciences of the United States of America*, *112*(37), E5218–E5218. https://doi.org/10.1073/pnas.1515511112

Huntzinger, D. N., Schwalm, C., Michalak, A. M., Schaefer, K., King, A. W., Wei, Y., et al. (2013). The North American Carbon Program Multi-Scale Synthesis and Terrestrial Model Intercomparison Project—Part 1: Overview and experimental design. *Geoscientific Model Development*, *6*, 2121–2133. https://doi.org/10.5194/gmd-6-2121-2013

Jacob, D. J., Turner, A. J., Maasakkers, J. D., Sheng, J., Sun, K., Liu, X., et al. (2016). Satellite observations of atmospheric methane and their value for quantifying methane emissions. *Atmospheric Chemistry and Physics*, *16*(22), 14, 371–14, 396. https://doi.org/10.5194/acp-16-14371-2016

Janjic, Z. (2002). Nonsingular implementation of the Mellor-Yamada level 2.5 scheme in the NCEP Meso model, Natl. Centers Environ. Predict., 61.

Kaplan, J. (2002). Wetlands at the last glacial maximum: Distribution and methane emissions. *Geophysical Research Letters*, *29*(6), 1079–3-4. https://doi.org/10.1029/2001GL013366

Kim, S. Y., Millet, D. B., Hu, L., Mohr, M. J., Griffis, T. J., Wen, D., et al. (2013). Constraints on carbon monoxide emissions based on tall tower measurements in the U.S. upper Midwest. *Environmental Science & Technology*, *47*(15), 8316–8324. https://doi.org/10.1021/es4009486

Kort, E. A., Frankenberg, C., Costigan, K. R., Lindenmaier, R., Dubey, M. K., & Wunch, D. (2014). Four corners: The largest US methane anomaly viewed from space. *Geophysical Research Letters*, *41*, 6898–6903. https://doi.org/10.1002/2014GL061503

Lassey, K. R. (2007). Livestock methane emission: From the individual grazing animal through national inventories to the global methane cycle. *Agricultural and Forest Meteorology*, *142*(2-4), 120–132. https://doi.org/10.1016/j.agrformet.2006.03.028

Lin, J. C., Gerbig, C., Wofsy, S. C., Andrews, A. E., Daube, B. C., Davis, K. J., & Grainger, C. A. (2003). A near-field tool for simulating the upstream influence of atmospheric observations: The Stochastic Time-Inverted Lagrangian Transport (STILT) model. *Journal of Geophysical Research*, *108*(D16), 4493. https://doi.org/10.1029/2002JD003161

Lin, J. C., Gerbig, C., Wofsy, S. C., Andrews, A. E., Daube, B. C., Grainger, C. A., & Hollinger, D. Y. (2004). Measuring fluxes of trace gases at regional scales by Lagrangian observations: Application to the CO_2 Budget and Rectification Airborne (COBRA) study. *Journal of Geophysical Research*, *109*, D15304. https://doi.org/10.1029/2004JD004754

Maasakkers, J. D., Jacob, D. J., Sulprizio, M. P., Turner, A. J., Weitz, M., Wirth, T., et al. (2016). A gridded version of the EPA national methane inventory. *Environmental Science & Technology*, *50*(23), 13,123–13,133. https://doi.org/10.1021/acs.est.6b02878

Mesinger, F., DiMego, G., Kalnay, E., Mitchell, K., Shafran, P. C., Ebisuzaki, W., et al. (2006). North American regional reanalysis. *Bulletin of the American Meteorological Society*, *87*(3), 343–360. https://doi.org/10.1175/BAMS-87-3-343

Michalak, A. M., Randazzo, N. A., & Chevallier, F. (2017). Diagnostic methods for atmospheric inversions of long-lived greenhouse gases. *Atmospheric Chemistry and Physics*, *17*(12), 7405–7421. https://doi.org/10.5194/acp-17-7405-2017

Miller, S. M., Matross, D. M., Andrews, A. E., Millet, D. B., Longo, M., Gottlieb, E. W., & Wofsy, S. C. (2008). Sources of carbon monoxide and formaldehyde in North America determined from high-resolution atmospheric data. *Atmospheric Chemistry and Physics*, *8*(3), 11, 395–11, 451. https://doi.org/10.5194/acpd-8-11395-2008

Miller, S. M., Worthy, D. E. J., Michalak, A. M., Wofsy, S. C., Kort, E. A., Havice, T. C., et al. (2014). Observational constraints on the distribution, seasonality, and environmental predictors of north American boreal methane emissions. *Global Biogeochemical Cycles*, *28*, 146–160. https://doi.org/10.1002/2013GB004580

Miller, S. M., Wofsy, S. C., Michalak, A. M., Kort, E. A., Andrews, A. E., Biraud, S. C., et al. (2013). Anthropogenic emissions of methane in the United States. *Proceedings of the National Academy of Sciences of the United States of America*, *110*(50), 20,018–20,022. https://doi.org/10.1073/pnas.1314392110

Nehrkorn, T., Eluszkiewicz, J., Wofsy, S. C., Lin, J. C., Gerbig, C., Longo, M., & Freitas, S. (2010). Coupled Weather Research and Forecasting-stochastic time-inverted lagrangian transport (WRF-STILT) model. *Meteorology and Atmospheric Physics*, *107*(1-2), 51–64. https://doi.org/10.1007/s00703-010-0068-x

Nisbet, E. G. E., Dlugokencky, J., & Bousquet, P. (2014). Methane on the rise—again. *Science*, *343*(6170), 493–495. https://doi.org/10.1126/science.1247828

Olson, D., Griffis, T. J., Noormets, A., Kolka, R., & Chen, J. (2013). Interannual, seasonal, and retrospective analysis of the methane and carbon dioxide budgets of a temperate peatland. *Journal of Geophysical Research: Biogeosciences*, *118*, 226–238. https://doi.org/10.1002/jgrg.20031

Rodgers, C. D. (2000). *Inverse methods for atmospheric sounding: Theory and practice* (Vol. 2, p. 256). Singapore: World scientific. https://doi.org/10.1142/3171

Schroeder, R., McDonald, K. C., Chapman, B. D., Jensen, K., Podest, E., Tessler, Z. D., et al. (2015). Development and evaluation of a multi-year fractional surface water data set derived from active/passive microwave remote sensing data. *Remote Sensing*, *7*(12), 16,688–16,732. https://doi.org/10.3390/rs71215843

Simpson, I. J., Thurtell, G. W., Neumann, H. H., Den Hartog, G., & Edwards, G. C. (1998). The validity of similarity theory in the roughness sublayer above forests. *Boundary-Layer Meteorology*, *87*(1), 69–99. https://doi.org/10.1023/A:1000809902980

Sommer, S., Petersen, S., & Møller, H. (2004). Algorithms for calculating methane and nitrous oxide emissions from manure management. *Nutrient Cycling in Agroecosystems*, *69*(2), 143–154. https://doi.org/10.1023/B:FRES.0000029678.25083.fa

Turner, A. J., & Jacob, D. J. (2015). Balancing aggregation and smoothing errors in inverse models. *Atmospheric Chemistry and Physics*, *15*(12), 7039–7048. https://doi.org/10.5194/acp-15-7039-2015

Turner, A. J., Jacob, D. J., Wecht, K. J., Maasakkers, J. D., Lundgren, E., Andrews, A. E., et al. (2015). Estimating global and north American methane emissions with high spatial resolution using GOSAT satellite data. *Atmospheric Chemistry and Physics*, *15*(12), 7049–7069. https://doi.org/10.5194/acp-15-7049-2015

United States Department of Agriculture-National Agricultural Statistics Service (2014). Census of Agriculture, 2012. Technical Report 2014.

US Forest Service (2016). National Wetlands Inventory. Retrieved from http://www.fws.gov/wetlands

Vanderzaag, A. C., Flesch, T. K., Desjardins, R. L., Baldé, H., & Wright, T. (2014). Agricultural and forest meteorology measuring methane emissions from two dairy farms: Seasonal and manure-management effects. *Agricultural and Forest Meteorology*, *194*, 259–267. https://doi.org/10.1016/j.agrformet.2014.02.003

Wecht, K. J., Jacob, D. J., Frankenberg, C., Jiang, Z., & Blake, D. R. (2014). Journal of geophysical research: Atmospheres of SCIAMACHY satellite data. *Journal of Geophysical Research: Atmospheres*, *119*, 7741–7756. https://doi.org/10.1002/2014JD02155

Wei, Y., Liu, S., Huntzinger, D. N., Michalak, A. M., Viovy, N., Post, W. M., et al. (2014). The north American carbon program multi-scale synthesis and terrestrial model Intercomparison project—Part 2: Environmental driver data. *Geoscientific Model Development*, *7*(6), 2875–2893. https://doi.org/10.5194/gmd-7-2875-2014

Wood, J. D., Gordon, R. J., & Wagner-Riddle, C. (2013). Biases in discrete CH_4 and N_2O sampling protocols associated with temporal variation of gas fluxes from manure storage systems. *Agricultural and Forest Meteorology*, *171-172*, 295–305. https://doi.org/10.1016/j.agrformet.2012.12.014

Wood, J. D., Griffis, T. J., Baker, J. M., Frankenberg, C., Verma, M., & Yuen, K. (2016). Multi-scale analyses reveal robust relationships between gross primary production and solar induced fluorescence. *Geophysical Research Letters*, *44*, 533–541. https://doi.org/10.1002/2016GL070775

Zhang, X., Lee, X., Griffis, T. J., Baker, J. M., Erickson, M. D., Hu, N., & Xiao, W. (2014). The influence of plants on atmospheric methane in an agriculture-dominated landscape. *International Journal of Biometeorology*, *58*(5), 819–833. https://doi.org/10.1007/s00484-013-0662-y

Zhang, X., Lee, X., Griffis, T. J., Baker, J. M., & Xiao, W. (2014). Estimating regional greenhouse gas fluxes: An uncertainty analysis of planetary boundary layer techniques and bottom-up inventories. *Atmospheric Chemistry and Physics*, *14*(19), 10,705–10,719. https://doi.org/10.5194/acp-14-10705-2014